Langmuir

Article

pubs.acs.org/Langmuir

Single-Chain Polymers Achieved from Radical Polymerization under Single-Initiator Conditions

Shen Zhang,[†] Xiangchao Pang,[‡] Dameng Guo,[§] Bo Zheng,[§] Shuxun Cui,*[,‡] and Hongwei Ma*[,†]

[†]Division of Nanobiomedicine, Suzhou Institute of Nano-tech and Nano-bionics, Chinese Academy of Sciences, Suzhou 215123, PR China

[‡]Key Laboratory of Advanced Technologies of Materials (Ministry of Education), Southwest Jiaotong University, Chengdu 610031, PR China

[§]Department of Chemistry, Chinese University of Hong Kong, Shatin, Hong Kong, PR China

Supporting Information

ABSTRACT: Radical polymerization from a single initiator molecule in a microenvironment is a nearly ideal system in which bimolecular termination, solution concentration, and viscosity changes could be neglected. In this study, we provide two facile methods of preparing polymers via atom-transfer radical polymerization (ATRP) under single-initiator conditions: tether initiators on planar substrates at superlow density through mixed self-assembled monolayers (SAMs) and encapsulated single initiators in microfluidic droplets. The molecular weight (MW) of the resultant polymers characterized by atomic force microscope-based single-molecule force spectroscopy (AFM-based SMFS) showed that the single-chain ATRP had an extraordinarily faster chain propagation rate (2 unit/s) on planar substrates and gave polymers with much higher MWs (10^5–10^6 g/mol) than those obtained from traditional ATRP (10^3–10^5 g/mol). The former method offered a general platform for single-chain polymer synthesis and investigation, and the latter could be amplified to obtain abundant single-chain polymers with ultrahigh molecular weight (UHMW) for commercial applications.

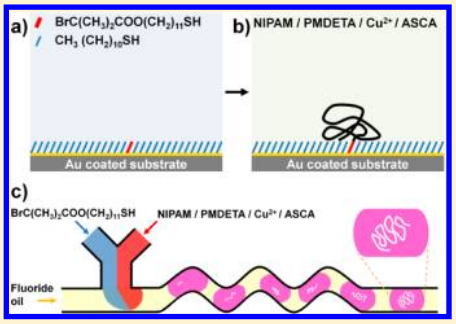

INTRODUCTION

Benefitting from the continuous emergence of novel synthesis and characterization strategies, polymers can be imaged,[1] synthesized,[2,3] tailored,[4] assembled,[5] and manipulated[6] on the molecular level, which is the key to the generation of unimolecular devices.[7] Single-chain objects were mostly obtained from ultradilute solutions or synthesized under dilute conditions,[8,9] which needs improvement in controllability and repeatability. Herein, we provide two facile methods of preparing single-chain polymers via ATRP under single-initiator conditions: tether initiators on planar substrates at superlow density through mixed SAMs and encapsulated single initiators in microfluidic droplets (Scheme 1). Single-initiator conditions could be considered to be a nearly ideal system in which bimolecular termination, solution concentration, and viscosity changes could be neglected. Radical polymerization under the above two kinds of conditions predictably results in single-chain polymers with ultrahigh molecular weight. To investigate single-chain polymers, atomic force microscope-based single-molecule force spectroscopy (AFM-based SMFS) was used to characterize the length of each chain in the stretching stage. The MW converted from chain length showed the single-chain ATRP conducting on planar substrates and gave polymers with much higher MWs than those obtained from traditional ATRP (10^3–10^5 g/mol).[10,11] The single-chain ATRP conducted in microfluidic droplets resulted in single-chain polymers with larger dimensions and more narrow distributions. The former method gave a general platform for single-polymer-chain investigation, and the latter could be amplified to obtain abundant UHMW polymers using parallel microfluidic devices.[12] Our study will be a valuable addition to the polymer synthesis repertoire.

EXPERIMENTAL SECTION

Materials and Sample Preparation. The initiator thiol (ω-mercaptoundecyl bromoisobutyrate, I), diluent thoil (1-undecanethiol, UDT), and Au-coated substrates (80 nm Au with a 5 nm chrome adhesion layer on quartz, by thermal evaporation in vacuum) were received from Suzhou Hongrong Biotechnology Co. Ltd. (China) as gifts. Monomer *N*-isopropylacrylamide (NIPAM, TCI Corp., Japan) was recrystallized twice from benzene/hexane (3:2 v/v) and dried in vacuum before use. All chemicals were analytically pure and used without further treatment, if not mentioned otherwise. Deionized (DI) water (>15 MΩ) was used when water was involved.

Methods. Planar substrates of superlow initiator density were prepared as follows: Au-coated quartz substrates were cleaned with UV/ozone (ProCleaner, Bioforce Nanosciences, Inc.) for 30 min and then rinsed with ethanol and dried with N_2. Then the substrates were immersed in a set of mixed thiol solutions in ethanol for 15 h, which had gradient molar ratios of initiator (χ_I, $\chi_I = M_I/[M_I + M_{UDT}]$) of 10^{-3}, 10^{-6}, 10^{-9}, and 10^{-12}. The total thiol concentration was 1 mM

Received: August 2, 2012
Revised: September 12, 2012
Published: October 8, 2012

Scheme 1. Single-Chain ATRP Realized on a Planar Surface and in Microdroplets[a]

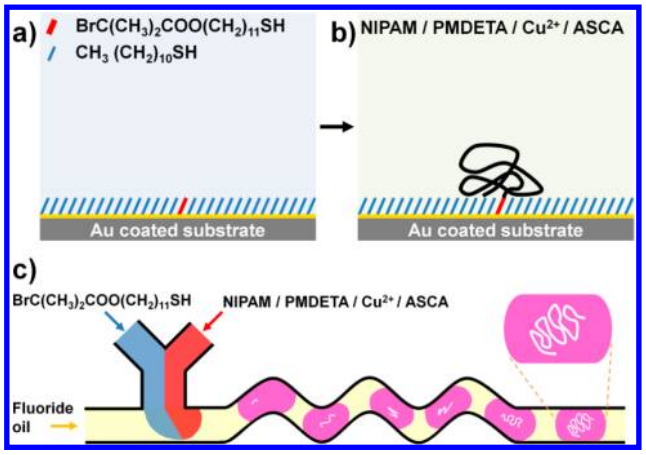

[a](a) Single-initiator conditions realized through mixed SAMs from the superlow initiator density ($\chi_I = 10^{-12}$) on a Au-coated substrate. (b) Surface-initiated polymerization gave isolated polymer chains with a surface density of $\sim 10^{-7}$ chain/nm^2. (c) Single-chain ATRP conducted in microfluidic droplets. The initiator concentration was as low as 0.1 fM to make sure that there was one or zero initiator in each droplet.

for each solution. The resultant binary mixed SAM-coated substrates were subjected to ATRP to generate poly(*N*-isopropyl-acrylamide) (PNIPAM).

The standard ATRP solution was prepared as follows: NIPAM (0.8 g, 7.1 mM) was dissolved in a mixture of methanol (6 mL) and water (2.46 mL, Milli-Q) and degassed by bubbling with Ar for 30 min. Solutions of $CuCl_2$ (1.77 mL, 0.04 M), *N*,*N*,*N*′,*N*″,*N*″-pentamethyl-diethylenetriamine (PMDETA, 29.52 μL), and ascorbic acid (ASCA, 1.77 mL, 0.04 M) were added to this solution in sequence. The mixture was then stirred and bubbled for another 30 min. ATRP was conducted in a glovebox (oxygen content <0.1 ppm) by adding 2 mL of the reaction mixture to each substrate individually. After various durations, polymerization was terminated by removing the substrates from the reaction solution and immediately placing them in water for cleaning. Purification was accomplished by thoroughly rinsing the substrates with water and ethanol and finally drying them in a stream of N_2.

In microfluidic synthesis, a 0.1 fM initiator solution was used, and the concentrations of monomer and catalysts in solution were twice as much as those in a standard ATRP solution. The initiator solution, monomer/catalysts solution, and fluorocarbon oil (3M fluorinert FC-3283) were all bubbled with Ar for 1 h. The flow rates of the above-mentioned solutions were 1, 1, and 8 μL/min, respectively. The generated droplets were imported into poly(tetrafluoroethylene) tubes with an inner diameter of 300 μm and then remained in the tubes for 12 h to conduct ATRP at RT under an Ar atmosphere. The final volume of the droplets was about 20 nL. As a result, there was one or zero initiator in each droplet, and the concentrations of monomer and catalysts in the droplets were the same as in the standard ATRP system. After polymerization, the droplets were exported and directly dropped onto copper grids for TEM observation. More droplets were collected in solution for AFM-SMFS characterization. Cleaned Au-coated substrates were immersed in the solution for 30 min and then rinsed with ethanol and water before the SMFS experiment. Initiator solutions (0.1 μM–0.1 mM, n_I (number of initiator molecules per droplet) = 10^6–10^{12} per droplet) were also used for comparison, and the resultant droplets were collected in solutions and further diluted 10^3-fold before immersion treatment.

Characterization. All of the tapping-mode AFM images of surface-tethered PNIPAM chains were obtained by using a Vecco Dimension 3100 in air at room temperature. A new AFM tip (NSC15/AIBS, Mikromash, tip radius <10 nm) was used for each test. The diameter and height of dots were measured by analyzing the cross-sectional profile from AFM images. Samples used in transmission electron microscopy (TEM, Tecnai G2 F20 S-Twin) observations were prestained with OsO_4 vapor for 15 min and vacuum dried at 50 °C for 3 days. Diameter distributions of globules were statistically analyzed by ImageJ 1.44p (n > 100).

Extension–force curves of the surface-tethered or adsorbed PNIPAM chains were obtained by using an MFP-3D AFM (Asylum Research, CA) at room temperature (RT, 23 ± 2 °C). Prior to the force measurements, the PNIPAM sample was immersed in water. Then the Au-coated Si_3N_4 AFM tip (NPG-10, tip radius of 30–60 nm, Bruker Corp., CA) was set to capture and stretch the PNIPAM chain from random sites in water at room temperature (3 samples for each group, 20 sites on one sample, and more than 200 times for each site). The data was collected at the same time and converted to force–extension curves. The spring constant of the cantilevers was measured by a thermoexcitation method and ranged from 40 to 60 pN/nm. The stretching velocity applied in this study is 1.0 μm/s in automated mode. The maximum value and distribution of the chain extension (i.e., the bridging length, L_b) for each group were calculated and statistically analyzed by using maximum values taken from each testing site.

RESULTS AND DISCUSSION

Single-Chain ATRP Conducted on a Surface. Surface-initiated ATRP (SI-ATRP) was initially designed to prepare high-density polymer brushes on solid surfaces for a spectrum of applications.[13−15] We recently demonstrated that ATRP from substrates with a low initiator density also gave functional surface layers for biosensor or protein microarrays.[16−18] We reasoned that the single-initiator condition could be created if we lower the initiator density further. Therefore, we immersed the Au-coated substrates into a set of mixed thiol solutions that had gradient ratios of initiator to undecanethiol ($\chi_I = M_I/[M_I + M_{UDT}]$). The resultant mixed SAMs were subjected to ATRP to generate poly(*N*-isopropyl-acrylamide) (PNIPAM), which was selected as the model polymer for its relatively strong interaction with the Au-coated AFM tip. Tapping-mode AFM revealed the morphological changes in graft PNIPAM with the reduction of initiator density under the same ATRP conditions (Figures 1 and S1–S3). The coverage of PNIPAM on the

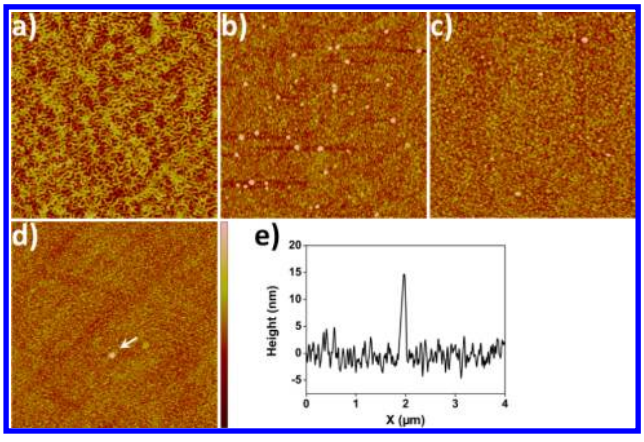

Figure 1. Morphological study of PNIPAM chains grafted from Au-coated substrates with different initiator densities. (a–d) Tapping-mode AFM images (4 μm × 4 μm scan size, 20 nm height) of PNIPAM prepared via 4 h of ATRP from substrates with $\chi_I = 10^{-3}$ (a), 10^{-6} (b), 10^{-9} (c), and 10^{-12} (d). (e) Section profile of the single PNIPAM chain in image d (indicated by the arrow). The height difference helped us to distinguish the single PNIPAM chain from the substrate. It indicated that single-chain ATRP was achieved at $\chi_I = 10^{-12}$.

dx.doi.org/10.1021/la303129q | *Langmuir* 2012, 28, 14954–14959

surface changed from a continuous layer ($\chi_I \geq 10^{-3}$) to separate dots ($\chi_I \leq 10^{-6}$) and eventually to a single dot within the scanned area ($\chi_I = 10^{-12}$). According to the average distance (1.7 ± 0.4 μm, Figure S3) between neighboring dots, the chain growth from these isolated initiators would not interfere with each other. Therefore, we identified $\chi_I = 10^{-12}$ as the single-initiator condition for single-chain ATRP on Au-coated substrates. Furthermore, purification of the graft single-chain PNIPAM could be easily realized by thoroughly rinsing.

When AFM-based SMFS was used,[19−25] the single polymer chain could be stretched between the substrate and AFM tip, and the MW could be calculated from the maximum value of the chain extension (also named the bridging length, L_b) using the fully extended chain model with a unit length of 0.25 nm (Figure S5).[26] However, given the randomness of the position of polymer chains where the tip was picked, most obtained L_b/MW values were shorter/smaller than the true values. Therefore, we applied statistical analysis to seek regularities, especially the trend in MW change as the polymerization condition was varied, namely, χ_I, time, monomer concentration ([M]), and catalyst concentration (represented by $[Cu^{2+}]$ and the initial ratio of $[Cu^{2+}]$ to ASCA was constant at 1:1, Figure 2). For comparison, each time we varied only one or two of the parameters while maintaing the others at standard conditions: $\chi_I = 10^{-12}$, t = 4 h, [M] = 590 mM, and $[Cu^{2+}]$ = 5.9 mM.

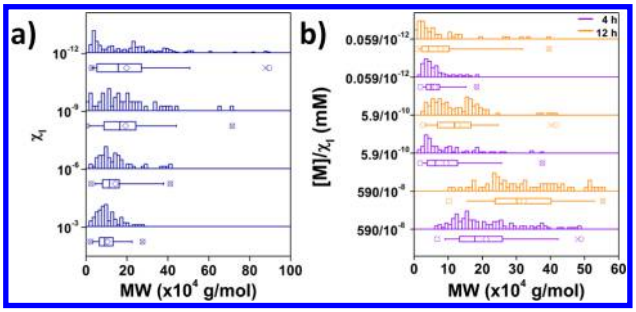

Figure 2. MW of PNIPAM chains was responsive to χ_I and [M]. (a) MW increased as χ_I decreased from 10^{-3} to 10^{-12}, and other ATRP conditions were fixed as the standard conditions. Shifts toward higher values indicated the increase in PNIPAM chain lengths with the decrease in χ_I. (b) MW variations as [M] and time change while [M]/χ_I was kept constant. Single-chain polymers with a high MW ($\sim 4 \times 10^5$ g/mol) were still obtained from the $0.0059/10^{-12}$ group after 12 h of polymerization. The data subjected to statistical analysis were the calculated MWs using maximum values taken from each testing site (n_{sample} = 3 for each group, n_{site} = 20 for each sample, and $n_{SMFS} \geq 200$ for each site). Histograms and box charts were used to represent the distribution and maximum value of MW for each group. Representative values in box charts from left to right were the minimum (○), median (I), mean (◊), maximum (○), and 5th(×)/25th (I-)/75th (-I)/95th (×) percentile, respectively.

We investigated the MW of PNIPAM chains from substrates with different χ_I values while other ATRP conditions were kept constant (Figure 2a). As the initiator density decreased from χ_I of 10^{-3} to 10^{-12}, the maximum MW increased from 2.7×10^5 to 9.0×10^5 g/mol (Table S1). Although obtaining the maximum L_b was a small probability event, this was the closest value to real MW. A similar trend was also found for the average values of MW (Table S1, Figure 2a), indicating that ATRP from the substrate with a lower initiator density resulted in a higher MW. Brooks et al. reported that the MW estimated from L_b was comparable to that determined by GPC for high-density polymer brushes. However, MW estimated from L_b was smaller (by ~60%) than that determined by GPC as the decrease in polymer density from 0.171 to 0.0125 chain/nm^2.[26] Given the superlow initiator density for SI-ATRP, it is reasonable to expect a much greater MW for the above-mentioned four samples. This set of data (Figure 2a) also highlighted how dramatically the bimolecular termination reaction affected the MW distribution. Both theoretical analysis and experimental observations confirmed that the growing sites (activated initiators) decreased as ATRP progressed, especially when the initial initiator density was high.[13−15] Such a reduction was mainly attributed to the bimolecular termination reaction among the closely packed initiators, which in turn limited the MW of most surface-grafted polymer chains. As the bimolecular termination reaction that would lead to the reduction of initiator density from χ_I of 10^{-3} to 10^{-12} on the same substrate as ATRP progressed, rare long chains would be buried in abundant short chains. Thus, long chains that formed at a relatively higher initiator density were hardly detected.

The degree of polymerization is considered to be determined by the ratio of monomer to initiator for typical ATRP. However, things become quite different when polymerization is conducted on the surface. Compared to the total amount of initiators on substrates, the monomers in SIP solution were present in great excess. Thus, it was considered that the monomer concentration has not changed during SIP. If the reactants diffuse fast enough near the surfaces, then all active chains would grow at the same rate for each group. The differences in MW/chain length were found, though the [M]/χ_I values were kept constant as shown in Figure 2b. In general, the polymer chain did not form in a short time because there were significant increases in MW for each group after 4 h of polymerization. MW differences among the groups with 4 h of polymerization were mainly attributed to the monomer concentration change. The $0.0059/10^{-12}$ group still underwent fast chain propagation although the initiator and monomer concentrations were 1% and 1/10 000 of the other two groups, respectively. After 12 h, the MW of the $0.0059/10^{-12}$ group was similar to that of the $5.9/10^{-10}$ group. The possible reason for this could be the prolonged active-site lifetime without biomolecular termination under single-initiator conditions, which was named the single-initiator effect.

Second, we investigated the MW of PNIPAM as a function of time (Figure 3a). For t < 12 h, the MW statistics continued to rise as the time increased. For $t \geq 12$ h, there was no significant difference in MW. Such a trend was similar to the layer thickness development of regular SI-ATRP (i.e., from the high-density initiator layer), which was attributed to the fact that polymerization was quenched by leaking oxygen after a long time or because of side reactions.[15] Although we observed an MW increase as the time increased, currently no conclusion could be drawn on whether single-chain ATRP was living/controlled. The reversible termination of propagating radicals with $[Cu^+]/[Cu^{2+}]$ indeed worked, but there could be no equilibrium because there was only one initiator within the local area.

We also studied the effects of [M] and $[Cu^{2+}]$ on single-chain ATRP. Compared to the total number of initiators on the substrates (~2 fmol on a ϕ 12 mm Au-coated substrate theoretically), the monomers in solution were present in great excess. It was considered that the monomer concentration was almost constant throughout the single-chain ATRP. However, Figure 3b showed that the MW was sensitive to the change in

dx.doi.org/10.1021/la303129q | Langmuir 2012, 28, 14954−14959

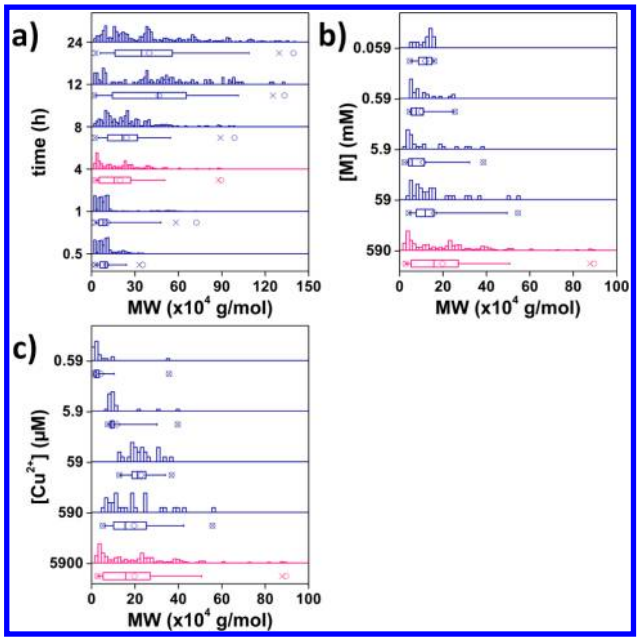

Figure 3. MW of PNIPAM chains as a function of time, [M], and [Cu^{2+}]. Note that the pink curve serves as the reference, which was a result of the standard conditions: $\chi_I = 10^{-12}$, t = 4 h, [M] = 590 mM, and [Cu^{2+}] = 5900 μM. (a) MW increased as time increased from 0 to 24 h. (b) MW decreased as [M] decreased from 590 to 0.059 mM. (c) MW decreased as [Cu^{2+}] decreased from 5900 to 0.59 μM. The data subjected to statistical analysis were the calculated MWs using the maximum values taken from each testing site (n_{sample} = 3 for each group, n_{site} = 20 for each sample, and $n_{SMFS} \geq 200$ for each site). Statistical values are also represented. Shifts toward higher values indicated an increase in the PNIPAM chain lengths with a decrease in χ_I and an increase in T, [M], or [Cu^{2+}].

To process a large number of samples, we applied the automated SMFS mode. However, in the manual SMFS mode, we found that the maximum L_b for the χ_I of the 10^{-12} group reached 6 μm (Figure 4), implying that the MW was no less

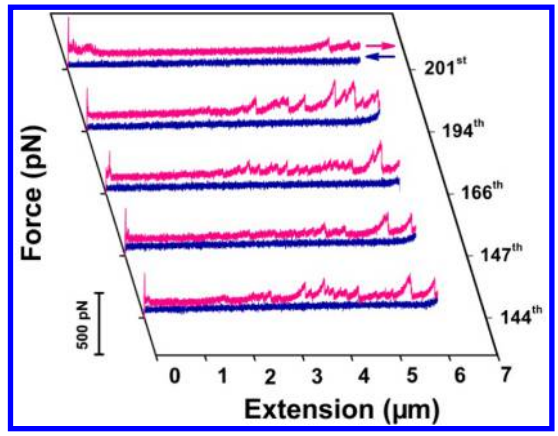

Figure 4. Representative force−extension curves with L_b larger than 6 μm for a single PNIPAM chain prepared via 4 h of ATRP from a substrate with $\chi_I = 10^{-12}$. These curves were obtained from the same position sequentially at the 144th, 147th, 166th, 194th, and 201st approaches (pink) and retractions (blue) of the AFM tip. The 201st curve exhibited a typical single-chain force−extension curve. The sawtooth curves indicated that the chain had a looplike conformation with many contact points on the substrate and tip. To extend the chain as far as possible, the retraction speed of tip was turned down manually when a chain was captured. In this case, some of the initial forces in approaching curves did not return to zero (the right ends of red curves bend upward in the 144th, 147th, and 194th curves), which means that the captured chain had not yet desorbed completely from the tip in the last retraction. Thus, the full length of this PNIPAM chain was still longer than the measured range.

[M] and fell by a quarter as [M] decreased from 590 mM to 5.9 μM. Because the propagation was considered to continue during the first 4 h of reaction, the MW of the obtained polymers and the propagation rate should be proportional to the monomer concentration. We attributed the abnormal observation to the drawback of SMFS: the longer the chain, the harder it was to stretch it fully. Compared to varying time, controlling [M] was a better way to tune the MW of single-chain polymers. Similarly, compared to the total number of initiators on substrates, [Cu^{2+}] was also present in great excess. Figure 3c shows the decrease in MW as [Cu^{2+}] decreased from 5.9 mM to 59 μM, whereas there was no significant change in MW as [Cu^{2+}] decreased from 59 to 0.59 μM. Matyjaszewski et al. previously showed that the ratio between [Cu^{+}] and [Cu^{2+}] determined the polymerization, not the absolute concentration.[27] Although the ratio of [Cu^{+}] to [Cu^{2+}] did not change too much, the absolute concentration of them decreased. The durations of both chain propagation and the dormant state would be prolonged. It could be used to explain the unchanged MW with respect to catalysts after the first fall. This demonstrated that the reversible reaction still worked, although single-chain ATRP did not possess ATRP equilibrium. Here we propose that the possibility of collision was a function of molecular concentration (i.e., [M], [Cu^{+}], and [Cu^{2+}]). Detailed mechanistic studies such as varying the kinds of monomer, the ratio of [Cu^{+}]/[Cu^{2+}], and the solvent composition are currently under investigation and will be reported elsewhere.

than 2.6 × 10^6 g/mol, which is strong evidence for an ultrafast chain propagation rate for single-chain ATRP. Thus, single-chain ATRP might reveal the essential chain propagation ability of ATRP and also might highlight the bimolecular termination reaction in ATRP.

Single-Chain ATRP Conducted in Microfluidic Droplets. Before this single-chain ATRP becomes a valuable addition to the repertoire of polymer synthesis, one needs to realize the massive production of polymer from single-chain ATRP because this strategy causes a decrease in polymer production by 6 orders of magnitude. Here we applied droplet microfluidics to reproduce and amplify single-chain ATRP in solution.[28,29] The initiator used in microfluidic synthesis was the same as that in single-chain ATRP on planar substrates. In T-junction microfluidic synthesis, the initiator solution was diluted in 0.1 fM to ensure that there was <1 initiator in each droplet. The concentrations of NIPAM and catalysts in droplets were the same under the ATRP condition on Au-coated substrates. The resultant single-chain PNIPAM prepared from the n_I (number of initiator molecules per droplet) = 1 condition exhibited particles with diameters of 8.8 ± 1.5 nm under TEM (Figure 5d). The dimensions of the particles significantly decreased as n_I increased from 10^6 to 10^{12} (Figure 5a−c). Although the average diameter difference between the n_I values of 1 and 10^6 groups was small, the former exhibited a more narrow distribution. We assumed that the bimolecular termination reaction in the n_I of the 10^6 group was weaker than that in the n_I values of 10^9 and 10^{12} groups but still heavier than

dx.doi.org/10.1021/la303129q | Langmuir 2012, 28, 14954−14959

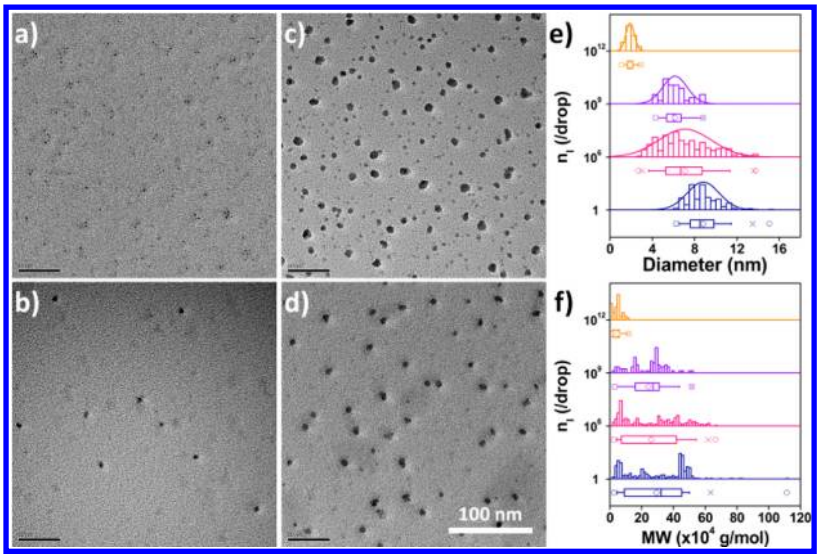

Figure 5. Morphological and MW characterization of single-chain PNIPAM prepared by single-chain ATRP in microfluidic droplets. (a–d) TEM images of typical single-chain PNIPAM particles prepared from n_I values of 1 (a), 10^6 (b), 10^9 (c), and 10^{12} (d) per droplet conditions by using the microfluidic system. The particles were supported by an ultrathin carbon film and stained with OsO_4. (e) Diameter distribution of PNIPAM particles as in images a–d. (f) MW of PNIPAM (a–d) evaluated by AFM-SMFS. Histograms and box charts were used to represent the distribution and maximum value of MW for each group. Statistical values were represented as those in Figure 2. Short chains of ~6.5×10^4 g/mol were mainly attributed to the self-polymerization in solution for 12 h.

that in the n_I of the 1 group. The MW evaluation of the above groups by AFM-SMFS showed that single-chain ATRP in droplets could generate single PNIPAM chains with MW of the same order of magnitude (Table S3, S6), indicating that the bimolecular termination reaction was also suppressed by conducting single-chain ATRP in microfluidic droplets. However, the capacity of our single-channel device was still far from the minimum required dose of the GPC test. We also grappled with technical difficulties in utilizing parallel devices, which will be discussed comprehensively in another article. Although the dimerization of thiol-terminated PNIPAM could double the length of the PNIPAM chain, it will not change the SMFS results because this doubled chain will be fixed to the Au surface by two Au–S bonds.

■ CONCLUSIONS

We realized single-chain ATRP on planar substrates and in microfluidic droplets. AFM-based SMFS revealed that such single-initiator conditions could lead to ultrafast polymerization (2 unit/s) and UHMW (10^5–10^6 g/mol), which was named the single-initiator effect. The main reason for this single-initiator effect is the elimination of bimolecular termination by the physical isolation of growing sites. It would be interesting to study the ATRP process for a single initiator over a local area.

■ ASSOCIATED CONTENT

Ⓢ Supporting Information

Morphology characterization by AFM and MW characterization by AFM-based SMFS. This material is available free of charge via the Internet at http://pubs.acs.org.

■ AUTHOR INFORMATION

Corresponding Author

*E-mail: cuishuxun@swjtu.edu.cn (for MW characterization by AFM-SMFS) and hwma2008@sinano.ac.cn (for single-chain ATRP).

Author Contributions

H.M. and S.Z. designed this project. S.Z. conducted most of the SI-ATRP experiments. X.P. performed most of the AFM measurements. S.Z. and D.G. conducted the microfluidic experiments. S.Z., S.C., and H.M. analyzed the data and wrote the article.

Notes

The authors declare no competing financial interest.

■ ACKNOWLEDGMENTS

This work was supported by the National Natural Science Foundation of China (21104092 and 21074148). We thank Prof. H. Y. Zhao and Dr. Y. Shao for helpful discussions and technical assistance. We acknowledge the electroscope support of the Public Center for Characterization and Test, SINANO, CAS.

■ REFERENCES

(1) Roiter, Y.; Minko, S. AFM single molecule experiments at the solid-liquid interface: in situ conformation of adsorbed flexible polyelectrolyte chains. *J. Am. Chem. Soc.* **2005**, *127*, 15688–15689.

(2) Okawa, Y.; Aono, M. Materials science: nanoscale control of chain polymerization. *Nature* **2001**, *409*, 683–684.

(3) Sakaguchi, H.; Matsumura, H.; Gong, H.; Abouelwafa, A. M. Direct visualization of the formation of single-molecule conjugated copolymers. *Science* **2005**, *310*, 1002–1006.

(4) Ida, S.; Terashima, T.; Ouchi, M.; Sawamoto, M. Selective radical addition with a designed heterobifunctional halide: a primary study toward sequence-controlled polymerization upon template effect. *J. Am. Chem. Soc.* **2009**, *131*, 10808–10809.

(5) Liu, X.; Jin, X.; Peter, X. M. Nanofibrous hollow microspheres self-assembled from star-shaped polymers as injectable cell carriers for knee repair. *Nat. Mater.* **2011**, *10*, 398–406.

(6) Duwez, A.; Cuenot, S.; Jerome, C.; Gabriel, S.; Jerome, R.; Rapino, S.; Zerbetto, F. *Nat. Nanotechnol.* **2006**, *1*, 122–125.

(7) Ouchi, M.; Badi, N.; Lutz, J.; Sawamoto, M. Single-chain technology using discrete synthetic macromolecules. *Nat. Chem.* **2011**, *3*, 917–924.

(8) Harth, E.; Horn, B. V.; Lee, V. V.; Germack, D. S.; Gonzales, C. P.; Miller, R. D.; Hawkere, C. J. A facile approach to architecturally defined nanoparticles via intramolecular chain collapse. *J. Am. Chem. Soc.* **2002**, *124*, 8653−8660.
(9) Foster, E. J.; Berda, E. B.; Meijer, E. W. Metastable supramolecular polymer nanoparticles via intramolecular collapse of single polymer chains. *J. Am. Chem. Soc.* **2009**, *131*, 6964−6966.
(10) Xia, Y.; Yin, X.; Burke, N. A. D.; Stöver, H. D. H. Thermal response of narrow-disperse poly(*n*-isopropylacrylamide) prepared by atom transfer radical polymerization. *Macromolecules* **2005**, *38*, 5937−5943.
(11) Masci, G.; Giacomelli, L.; Crescenzi, V. Atom transfer radical polymerization of n-isopropylacrylamide. *Macromol. Rapid Commun.* **2004**, *25*, 559−564.
(12) Zeng, Y.; Novak, R.; Shuga, J.; Smith, M. T.; Mathies, R. A. High-performance single cell genetic analysis using microfluidic emulsion generator arrays. *Anal. Chem.* **2010**, *82*, 3183−3190.
(13) Edmondson, S.; Osborne, V. L.; Huck, W. T. S. Polymer brushes via surface-initiated polymerizations. *Chem. Soc. Rev.* **2004**, *33*, 14−22.
(14) Barbey, R.; Lavanant, L.; Paripovic, D.; Schuwer, N.; Sugnaux, C.; Tugulu, S.; Klok, H. A. Polymer brushes via surface-initiated controlled radical polymerization: synthesis, characterization, properties, and applications. *Chem. Rev.* **2009**, *109*, 5437−5527.
(15) Ma, H.; Wells, M.; Beebe, T. P.; Chilkoti, A. Surface-initiated atom transfer radical polymerization of oligo(ethylene glycol) methyl methacrylate from mixed self-assembled monolayer on gold. *Adv. Funct. Mater.* **2006**, *16*, 640−648.
(16) Wu, Y.; Huang, Y.; Ma, H. A facile method for permanent and functional surface modification of poly(dimethylsiloxane). *J. Am. Chem. Soc.* **2007**, *129*, 7226−7227.
(17) Qian, T.; Li, Y.; Wu, Y.; Zheng, B.; Ma, H. Superhydrophobic poly(dimethylsiloxane) via surface-initiated polymerization with ultra-low initiator density. *Macromolecules* **2008**, *41*, 6641−6645.
(18) Ma, H.; He, J.; Liu, X.; Gan, J.; Jin, G.; Zhou, J. Surface initiated polymerization from substrates of low initiator density and its applications in biosensors. *ACS Appl. Mater. Interfaces* **2010**, *2*, 3223−3230.
(19) Bemis, J. E.; Akhremitchev, B. B.; Walker., G. C. Single polymer chain elongation by atomic force microscopy. *Langmuir* **1999**, *15*, 2799−2805.
(20) Hugel, T.; Grosholz, M.; Clausen−Schaumann, H.; Pfau, A.; Gaub, H. E.; Seitz, M. *Macromolecules* **2001**, *34*, 1039−1047.
(21) Cui, S.; Liu, C.; Zhang, W; Zhang, X.; Wu, C Desorption force per polystyrene segment in water. *Macromolecules* **2003**, *36*, 3779−3782.
(22) Sonnenberg, L.; Luo, Y.; Schlaad, H.; Seitz, M.; Colfen, H.; Gaub, H. E. Quantitative single molecule measurements on the interaction forces of poly(L-glutamic acid) with calcite crystals. *J. Am. Chem. Soc.* **2007**, *129*, 15364−15371.
(23) Cui, S.; Liu, C.; Zhang, X. Simple method to isolate single polymer chains for the direct measurement of the desorption force. *Nano Lett.* **2003**, *3*, 245−248.
(24) Cao, Y.; Lam, C.; Wang, M.; Li, H. Nonmechanical protein can have significant mechanical stability. *Angew. Chem., Int. Ed.* **2006**, *45*, 642−645.
(25) Janshoff, A.; Neitzert, M.; Oberdorf, Y.; Fuchs, H. Force spectroscopy of molecular systems-single molecule spectroscopy of polymers and biomolecules. *Angew. Chem., Int. Ed.* **2000**, *39*, 3212−3237.
(26) Goodman, D.; Kizhakkedathu, J. N.; Bbrooks, D. E. Evaluation of an atomic force microscopy pull-off method for measuring molecular weight and polydispersity of polymer brushes: effect of grafting density. *Langmuir* **2004**, *20*, 6238−6245.
(27) Matyjaszewski, K.; Xia, J. Atom transfer radical polymerization. *Chem. Rev.* **2001**, *101*, 2921−2990.
(28) Wu, T.; Mei, Y.; Cabral, J. T.; Xu, C.; Beers, K. L. A new synthetic method for controlled polymerization using a microfluidic system. *J. Am. Chem. Soc.* **2004**, *126*, 9880−9881.
(29) Quevedo, E.; Steinbacher, J.; McQuade, D. T. Interfacial polymerization within a simplified microfluidic device: capturing capsules. *J. Am. Chem. Soc.* **2005**, *127*, 10498−10499.